Bioorganic Chemistry 58 (2015) 72–80

Contents lists available at ScienceDirect

Bioorganic Chemistry

journal homepage: www.elsevier.com/locate/bioorg

Monoamine oxidase inhibitory activity of 2-aryl-4H-chromen-4-ones

Badavath Vishnu Nayak [a,1], S. Ciftci-Yabanoglu [b,1], Soumendranath Bhakat [c,1], Ajay Kumar Timiri [a], Barij N. Sinha [a], G. Ucar [b], Mahmoud E.S. Soliman [c], Venkatesan Jayaprakash [a,d,*]

[a] Department of Pharmaceutical Sciences and Technology, Birla Institute of Technology, Mesra, Ranchi, Jharkhand 835 215, India
[b] Department of Biochemistry, Faculty of Pharmacy, Hacettepe University, Sıhhiye 06100, Ankara, Turkey
[c] School of Health Sciences, University of KwaZulu-Natal, Westville, Durban 4001, South Africa
[d] Valens Pharma Services, Regus Citi Centre, Level 6, Chennai Citi Centre, 10/11, Dr. Radhakrishnan Salai, Chennai, Tamil Nadu 600 004, India

ARTICLE INFO

Article history:
Received 6 September 2014
Available online 3 December 2014

Keywords:
Human monoamine oxidase
Flavones
Enzyme inhibitors
Molecular docking
Molecular dynamics

ABSTRACT

A series of twenty 2-aryl-4H-chromen-4-one (flavones) derivatives (**3a–3s**) were synthesized and tested for hMAO inhibitory activity. Fifteen compounds (**3a**, **3c**, **3e**–**3h**, **3j**–**3p**, **3r**, **3s**) were found to be selective towards MAO-B, while **3d** was selective towards MAO-A, and **3b**, **3i** and **3q** were non-selective. Experimental Selectivity Index for MAO-B ranges from 2.0 (**3g**, **3p**) to 30.0 (**3j**). Compound **3j**, which is carrying 3,4-di-OMeC_6H_3 groups at R position on the molecule, was found to be potent MAO-B inhibitor amongst the fifteen with K_i value for MAO-B of 0.16 ± 0.01 μM comparable to that of standard drug, Selegiline (K_i for MAO-B is 0.16 ± 0.01 μM). Compound **3j** also appeared as the most selective MAO-B inhibitor according to its best selectivity index (30.0), which is comparable to that of Selegiline (SI_{MAO-B} = 35.0). Molecular docking and molecular dynamics simulation studies were carried out using Autodock-4.0 and Amber12 to understand the molecular level interaction and energy relation of MAO isoforms with selective inhibitors (**3d** and **3j**). Simulation results are in good agreement with the experimental results. Leads identified may further be explored to develop potent isoform specific inhibitors of MAO.

1. Introduction

Monoamine oxidases are responsible for the oxidative deamination of neurotransmitters and dietary amines. They contain flavin-adenosine-dinucleotide (FAD) as co-enzyme and are located on the outer mitochondrial membrane. There exists two different isoform, MAO-A and MAO B, classified based on their specificity towards their substrate and their selective inhibitors [1,2]. Serotonin, adrenaline and noradrenaline are substrates for MAO-A, while dopamine, phenylethylamine and benzylamine are substrates for MAO-B [2]. Iproniazide was the first drug approved for the treatment of depressive illness during 1950s and that was followed by imipramine, phenelzine, isocarboxazid and tranylcypromine. They were all found to be non-selective towards MAO isoforms as well as not specific towards peripheral and brain MAO. Due to which cheese-effect (Tyramine-induced hypertensive crisis) was reported with use of tranylcypromine during mid 1960s, leading to the establishment of strict dietary restrictions by US-FDA [3]. Tricyclic antidepressants and Selective Serotonin Reuptake Inhibitors emerged as an alternative to first generation antidepressants as they can be administered without any dietary restrictions [4]. Research during the past two decades clearly established the therapeutic utility of isoform selective and tissue specific MAO inhibitors in the treatment of depressive illness (MAO-A inhibitors) and neurodegenerative disorders (MAO-B inhibitors).

Chalcone derived pyrazolines were explored for their MAO inhibitory and antidepressant activity by many research groups. Few reports on MAO inhibitory activity [5–7] and antidepressant activity of chalcones [8–10] were also available. Flavones another oxygen containing heterocyclics derived from chalcones were also reported to exhibit antidepressant [11–13] and MAO-inhibitory activity [14–17]. Guided by these facts our group has synthesized a series of 2-aryl-4H-chromen-4-one (Flavones) and tested them for hMAO inhibitory activity.

2. Experimental

2.1. Materials and methods

Chemicals and solvents were of reagent grade and purchased from Sigma–Aldrich/Merck/CDH/Rankem. Completion of reaction

Abbreviations: MAO, monoamine oxidase; hMAO, human MAO; rMAO, rat MAO; SAR, structure–activity-relationship; bb, backbone; sc, side-chain.

* Corresponding author at: Department of Pharmaceutical Sciences and Technology, Birla Institute of Technology, Mesra, Ranchi, Jharkhand 835 215, India.
E-mail addresses: gulberk@hacettepe.edu.tr (G. Ucar), venkatesanj@bitmesra.ac.in (V. Jayaprakash).

[1] These authors contributed equally.

http://dx.doi.org/10.1016/j.bioorg.2014.11.008
0045-2068/

was monitored on TLC plates (Merck). Melting points were determined using OPTIMELT (Stanford Research System) and are uncorrected. Intermediates were characterized by their FT-IR spectra (FTIR-8400S-Schimadzu). Final compounds were characterized by their ^{1}H NMR (300 MHz, ECX-500, JEOL and 400 MHz, VNMRS400), ^{13}C NMR (400 MHz, VNMRS400), in either $CDCl_3$ or DMSO-d_6 as a solvent. The coupling constants (J) are expressed in hertz (Hz) and chemical shifts (δ) are reported in parts per million (ppm) units relative to TMS. Mass spectra of the final compounds were recorded by WATERS-Q-T of Premier-HAB213 using the ESI-MS Electro spray Ionization technique. Molecular modelling studies were carried using Maestro-8.5 (Schrodinger LLC) [18], AutoDock4 [19], Chimera [20] and Amber12 [21]. Microsoft Excel and Origin-6.0 were used for generating graphs. Molecular Docking studies were carried out on RHEL-5.0 Operating system installed on Dell Precision workstation with Intel core 2 quad processor and 8 GB RAM. While, Molecular dynamics (MD) simulations were run on a super computer taking in account 5 gpus. Molecules were prepared for MD simulation through PRODRG [22] and REDUCE [23] web servers.

2.2. Chemistry

2.2.1. General procedure for synthesis of Chalcones (**2a–2s**)

To a solution of 2′-hydroxy acetophenone (0.01 M) in ethanol (10 mL) an equimolar quantity of appropriate benzaldehydes was added and the mixture was maintained at <10 °C. Sodium hydroxide solution (60% in water) was added to the mixture drop wise with continuous stirring for a period of 30–45 min. The reaction mixture was then left at room temperature for about 48 h with occasional shaking. After 48 h, it was poured into ice-cold water and the pH was then adjusted to pH-2 using 6 N hydrochloric acid. The yellow precipitate obtained was filtered, washed with water and dried. The crude product was then recrystallized from methanol to give yellow product [24].

2.2.2. General procedure for the synthesis of flavones (**3a–3s**)

To a solution of Chalcones **(2a–2s**, 0.015 M) in 50 mL of dimethyl sulfoxide an equimolar quantity of iodine (0.015 M) was added. The reaction mixture was then stirred for about 30–60 min at 140 °C. The reaction mixture was then treated with aqueous sodium thiosulfate solution (20%) and extracted with chloroform (3 × 30 mL). The combined organic phase was then washed with brine, dried over anhydrous sodium sulphate and concentrated by in rotary evaporator. The residue was purified by recrystallization from suitable solvent to obtain desired final compounds (**3a–3t**) [25].

*2.2.2.1. 2-Phenyl-4H-chromen-4-one (**3a**).* Yield: 60%; mp: 95 °C (Lit. 96–97 °C) [26]; ^{1}H NMR (400 MHz, DMSO-d_6): δ (ppm) 7.0 (s, 1H, =C<u>H</u>—), 7.15 (d, 1H), 7.3 (t, 1H), 7.5 (t, 1H), 7.61 (m, 1H), 7.82 (m, 1H), 8.1 (m, 1H), 8.15 (d, 1H), 8.2 (m, 1H), 8.25 (d, 1H).

*2.2.2.2. 2-(2-Chlorophenyl)-4H-1-Benzopyran-4-one (**3b**).* Yield: 70%; mp: 195 °C (Lit. 192–193 °C) [25]; ^{1}H NMR (300 MHz, $CDCl_3$): δ (ppm) 6.63 (s, 1H, =C<u>H</u>—), 7.16 (t, 1H), 7.36–7.45 (m, 1H), 7.47–7.54 (m, 1H), 7.6 (d, 1H), 7.68 (t, 1H), 7.77 (d, 1H), 7.12 (d, 1H), 8.17–8.23 (m, 1H).

*2.2.2.3. 2-(4-Chlorophenyl)-4H-chromen-4-one (**3c**).* Yield: 65%; mp: 184 °C (Lit. 186–188 °C) [25]; ^{1}H NMR (300 MHz, $CDCl_3$): δ (ppm) 6.78 (s, 1H, =C<u>H</u>), 7.42 (t, 1H), 7.49 (d, 2H), 7.55 (d,1H), 7.69 (t, 1H), 7.82 (d. 2H), 7.19 (d,1H).

*2.2.2.4. 2-(2-Hydroxyphenyl)-4H-chromen-4-one (**3d**).* Yield: 55%; mp: 203 °C (Lit. 209–210 °C) [26]; ^{1}H NMR (400 MHz, DMSO-d_6): δ (ppm) 7.05 (m, 1H), 7.09 (s, 1H, =C<u>H</u>), 7.2 (t, 1H), 7.25 (t, 1H), 7.65 (m, 1H), 7.9 (m, 1H), 7.95 (d, 1H), 8.05 (d, 1H), 8.2 (d, 1H), 10.65 (s, 1H, -O<u>H</u>).

*2.2.2.5. 2-(3-Hydroxyphenyl)-4H-chromen-4-one (**3e**).* Yield: 40%; mp: 210 °C (Lit. 209–211 °C) [27]; ^{1}H NMR (300 MHz, DMSO-d_6) δ (ppm) 6.89 (s, 1H, =C<u>H</u>—), 7.28 (m, 1H), 7.4 (d,1H), 7.6 (t, 1H), 7.72 (t,1H), 7.83 (d, 1H), 8.16 (d, 1H), 8.24 (d,1H), 8.82 (s, 1H), 12.5 (s,1H, O<u>H</u>).

*2.2.2.6. 2-(4-Hydroxyphenyl)-4H-chromen-4-one (**3f**).* Yield: 50%; mp: 190 °C (Lit. 186–187 °C) [28]; ^{1}H NMR (400 MHz, DMSO-d_6) δ (ppm) 6.85 (s, 1H, =C<u>H</u>—), 6.94 (d, 2H), 7.47 (t, 1H), 7.73–7.80 (m, 1H), 7.95(d, 2H), 8.02(d, 1H), 8.4(d, 1H),10.38 (s, 1H, O<u>H</u>); ^{13}C NMR (400 MHz, DMSO-d_6) δ (ppm): 177.40, 163.59, 161.43, 156.0, 137.43, 134.51, 128.82, 125.79, 125.17, 123.73, 122.01, 118.81, 116.43, 105.24.

*2.2.2.7. 2-(2-Methoxyphenyl)-4H-chromen-4-one (**3g**).* Yield: 50%; mp: 136 °C (Lit. 129–130 °C) [26]; ^{1}H NMR (400 MHz, DMSO-d_6): δ (ppm) 3.9 (s, 3H, -OC<u>H</u>$_3$) 7.15 (d, 1H), 7.2 (m, 1H), 7.25 (m, 1H), 7.6 (m, 1H), 8.02 (d, 1H), 8.15 (m, 1H), 8.02 (s, 1H), 8.25 (d, 1H), 8.58 (d, 1H).

*2.2.2.8. 2-(3-Methoxyphenyl)-4H-chromen-4-one (**3h**).* Yield: 65%; mp: 125 °C (Lit. 130–131 °C) [29]; ^{1}H NMR (400 MHz, DMSO-d_6): δ (ppm) 3.8 (s, 3H, -OC<u>H</u>$_3$) 7.1 (s, 1H, =C<u>H</u>—), 7 (d, 1H), 7.5 (m, 2H), 7.62 (s, 1H), 7.7 (d, 1H), 7.82 (m, 2H), 8.03 (d, 1H).

*2.2.2.9. 2-(4-Methoxyphenyl)-4H-chromen-4-one (**3i**).* Yield: 60%; mp: 150 °C (Lit. 158–159 °C) [26]; ^{1}H NMR (400 MHz, $CDCl_3$): δ (ppm) 3.8 (s, 3H, OC<u>H</u>$_3$), 6.75 (s, 1H, =C<u>H</u>—), 7 (d, 2H), 7.4(t, 1H), 7.55 (d,1H), 7.6 (t,1H), 7.8 (d,2H), 8.25 (d,1H).

*2.2.2.10. 2-(3,4-Dimethoxyphenyl)-4H-chromen-4-one (**3j**).* Yield: 65%; mp: 167.5 °C (Lit. 175–176 °C) [26]; ^{1}H NMR (400 MHz, $CDCl_3$): δ (ppm) 3.8 (s, 3H, OC<u>H</u>$_3$), 3.99 (s, 3H, OC<u>H</u>$_3$), 6.7 (s, 1H, =C<u>H</u>—), 6.8 (s, 1H), 7 (d,1H), 7.39(t,1H), 7.4 (d,1H), 7.5 (d, 2H), 7.7 (m,2H), 8.2 (d,1H).

*2.2.2.11. 2-(4-Methylphenyl)-4H-chromen-4-one (**3k**).* Yield: 70%; mp: 106 °C (Lit. 110–111 °C) [26]; ^{1}H NMR (400 MHz, DMSO-d_6): δ (ppm) 2.2 (s, 1H, -C<u>H</u>$_3$), 7.0 (s, 1H, =C<u>H</u>), 7.25 (t, 1H), 7.4 (m, 2H), 7.45(t, 1H), 7.6 (m, 1H), 8–8.08 (m, 2H), 8.15 (d, 1H, -O<u>H</u>).

*2.2.2.12. 2-(4-Nitrophenyl)-4H-chromen-4-one (**3l**).* Yield: 60%; mp: 232 °C (Lit. 234–236 °C) [25]; ^{1}H NMR (300 MHz, $CDCl_3$): δ (ppm) 6.71 (s, 1H, =C<u>H</u>—), 7.1 (t, 1H), 7.38 (t, 1H), 7.49(d, 1H), 7.5 (d, 1H), 7.68 (m, 3H), 8.1 (dd, 1H); ESI-MS (m/z): Calculated 267.05, obsrevd 267.60 $(M+1)^+$.

*2.2.2.13. 4-(4-Oxo-4H-chromen-2-yl)benzonitrile (**3m**).* Yield: 60%; mp: 126 °C (Lit. 220–221 °C) [15]; ^{1}H NMR (300 MHz, $CDCl_3$): δ (ppm) 6.85 (s, 1H, =C<u>H</u>—), 7.42 (t, 1H), 7.55 (d, 1H), 7.71 (t, 1H), 7.8 (d, 2H), 8 (d, 2H), 8.2 (d, 1H); ESI-MS (m/z): Calculated, 247.06, observed 248.07 $(M+1)^+$.

*2.2.2.14. 2-(4-Bromophenyl)-4H-chromen-4-one (**3n**).* Yield: 60%; mp: 173 °C (Lit. 173–176 °C) [30]; ^{1}H NMR (300 MHz, $CDCl_3$) δ (ppm) 6.77 (s, 1H, =C<u>H</u>—), 7.4 (t, 1H), 7.55 (d, 1H), 7.64 (m, 3H), 7.77 (d, 2H), 8.2 (d, 2H); ESI-MS (m/z): Calculated 299.98, observed 300.50 $(M+1)^+$.

*2.2.2.15. 2-(Naphthalen-1-yl)-4H-chromen-4-one (**3o**).* Yield: 65%; mp: 105 °C; (Lit. 107–109 °C) [31]; ^{1}H NMR (300 MHz, $CDCl_3$): δ (ppm) 6.6 (s, 1H, =C<u>H</u>—), 4.5 (t, 1H), 7.56 (m, 2H), 7.68 (t, 1H),

7.2 (d, 1H), 7.9 (dd, 2H), 8 (d, 1H), 8.1 (dd, 2H), 8.2 (d, 1H); ESI-MS (*m*/*z*): 273.09 $(M+1)^+$.

*2.2.2.16. 2-(Naphthalen-2-yl)-4H-chromen-4-one (**3p**).* Yield: 63%; mp: 155.6 °C (Lit. 148–150 °C) [31]; ^{1}H NMR (300 MHz, $CDCl_3$): δ (ppm) 6.93 (s, 1H, =C<u>H</u>—), 8.4 (s, 1H), 7.22 (d, 1H), 7.9–7.8 (m, 4H), 7.69 (t, 1H), 7.61 (d, 1H), 7.59–7.52 (m, 2H), 7.4 (t, 1H); ESI-MS (*m*/*z*): Calculated 272.08, observed 273.09 $(M+1)^+$.

*2.2.2.17. 2-(Anthracen-9-yl)-4H-chromen-4-one (**3q**).* Yield: 70%; mp: 214 °C; ^{1}H NMR (300 MHz, $CDCl_3$): δ (ppm) 6.67 (s, 1H, =C<u>H</u>—), 7.47–7.54 (m, 6H), 7.7 (t, 1H), 7.95 (dd, 1H), 8.1 (dd, 2H), 8.4 (d, 1H), 8.6 (s, 1H); ^{13}C NMR (400 MHz, $CDCl_3$) δ (ppm) 116.2, 118.4, 124.2, 124.9, 125.5, 125.6, 125.9, 126.3, 127.3, 128.7, 129.8, 139.2, 131, 134, 157.3, 16.7, 178.05 ESI-MS (*m*/*z*): Calculated 322.10, observed 323$(M+1)^+$.

*2.2.2.18. 2-(Thiophen-2-yl)-4H-chromen-4-one (**3r**).* Yield: 56%; mp: 98 °C (Lit. 97–99 °C) [30]; ^{1}H NMR (300 MHz, $CDCl_3$): δ (ppm) 6.9 (s, 1H, =C<u>H</u>—), 7.48 (t, 1H), 7.6 (d, 1H), 7.75 (t, 1H), 8.1 (d, 1H), 8.24 (d, 1H), 8.37 (d, 2H); ESI-MS (*m*/*z*): Calculated 228.02, observed 228.60 $(M+1)^+$.

*2.2.2.19. 2-(Pyridin-3-yl)-4H-chromen-4-one (**3s**).* Yield: 50%; mp: 153 °C (Lit. 128–130 °C) [30]; ^{1}H NMR (300 MHz, $CDCl_3$): δ (ppm) 6.79 (s, 1H, =C<u>H</u>—), 7.35–7.49 (m, 2H), 7.5 (d, 1H), 7.6 (t, 1H), 8.12 (m, 2H), 8.7 (d, 1H), 9.1 (s, 1H); ESI-MS (*m*/*z*): Calculated 223.06, observed 223.60 $(M+1)^+$.

2.3. Biochemistry

2.3.1. Determination of hMAO-A and -B activities

The activities of recombinant hMAO-A and hMAO-B were determined using p-tyramine as common substrate and calculated as 0.18 ± 0.01 nmol/mg/min ($n = 3$) and 0.12 ± 0.02 nmol/mg/min ($n = 3$), respectively. The interactions of the synthesized compounds with hMAO isoforms were determined by a fluorimetric method described previously [28,32,33]. The production of H_2O_2 catalyzed by MAO isoforms was detected using a non-fluorescent Amplex®Red reagent which reacts with H_2O_2 in the presence of horseradish peroxidase to produce the fluorescent product resorufin. The reaction was started by the addition of 200 μM Amplex Red reagent, 1 U/mL horseradish peroxidase, and p-tyramine (concentration range 0.1–1 mM). Control experiments were carried out using reference inhibitors (Selegiline and Moclobemide). The possible capacity of compounds to modify the fluorescence generated in the reaction mixture due to non-enzymatic inhibition was determined by adding these compounds to solutions containing only the Amplex Red reagent in a sodium phosphate buffer.

2.3.2. Kinetic experiments

Synthesized compounds were dissolved in dimethylsulfoxide (DMSO), with a maximum concentration of 1%; in the concentration range of 1–100 μM. Kinetic data were determined using the Microsoft Excel package program. The slopes of the Lineweaver–Burk plots were replotted versus the inhibitor concentration, and the K_i values were determined from the *x*-axis intercept as $-K_i$. Each K_i value is the representative of single determination where the correlation coefficient (R^2) of the replot of the slopes versus the inhibitor concentrations was at least 0.98. The protein content was determined according to the Bradford method [34].

2.3.3. Reversibility experiments

Reversibility of the MAO inhibition with synthesized compounds was evaluated by a centrifugation-ultrafiltration method [35]. In brief, adequate amounts of the recombinant hMAO-A or B were incubated with a single concentration of the synthesized compounds or the reference inhibitors in a sodium phosphate buffer (0.05 M, pH 7.4) for 1 h at 37 °C. After this incubation period, an aliquot was stored at 4 °C and used for the measurement of MAO-A and -B activity. The remaining incubated sample was placed in an Ultrafree-0.5 centrifugal tube with a 30 kDa Biomax membrane and centrifuged at 9000× for 20 min at 4 °C. The enzyme retained in the 30 kDa membrane was resuspended in a sodium phosphate buffer at 4 °C and centrifuged again two successive times. After the third centrifugation, the enzyme retained in the membrane was resuspended in sodium phosphate buffer (300 mL) and an aliquot of this suspension was used for MAO-A and -B activity determination. Control experiments were performed simultaneously (to define 100% MAO activity) by replacing the inhibitors with appropriate dilutions of the vehicles. The corresponding values of percent (%) MAO isoform inhibition was separately calculated for samples with and without repeated washing.

2.4. Molecular docking simulation

In order to understand the molecular level interaction of the potent molecule **3d** and **3j** towards MAO-A and MAO-B, molecular docking studies were carried out using AutoDock4.0 [19]. Docking protocol reported earlier by our group has been followed with X-ray crystal structure of hMAO-A (2BXR) and hMAO-B (2BYB) downloaded from Protein Data Bank (www.rcsb.org) [36]. Protein preparation was carried out using Protein Preparation Wizard of Maestro-8.5 (Schrodinger LLC) [37]. Water and covalently linked ligands were deleted from the proteins and bond order was corrected for FAD. After assigning charge and protonation state, energy minimization was done using OPLS2005 force-field [38]. Ligands were prepared through PRODRG webserver (http://davapc1.bioch.dundee.ac.uk/cgi-bin/prodrg) [22]. For docking, grid parameter file (.gpf) and docking parameter files (.dpf) were written using MGLTools-1.4.6 [19]. Receptor grids were generated using 60 × 60 × 60 Grid points in *xyz* with grid spacing of 0.375 Å. Grid box was centered on N5 atom of FAD. Map types were generated using autogrid-4.0. Docking was carried out with following parameters: number of runs: 50, population size: 150, number of evaluations: 2,500,000 and number of generations: 27,000, using AutoDock4.0. Analysis of docking results was done using MGLTools-1.4.6. Top scoring molecule in the largest cluster was analyzed for its interaction with the protein.

2.5. Molecular dynamics simulation

In order to understand the stability and energetics of the docked complexes (compound **3d** complexed with MAO-A (PDB: 2BXR) and compound **3j** complexed with MAO-B (PDB: 2BYB), we prompted for a molecular dynamics simulation using GPU version of Amber12. The water molecules and all non-standard components were removed, making no changes in original co-ordinates. Missing hydrogens were further optimized using REDUCE server to generate a correct hydrogen bond network [23]. Chimera molecular modelling and visualization suite (https://www.cgl.ucsf.edu/chimera/) was used for structure preparation and visualization purpose [20]. All graphs were generated using Origin 6.0 data analysis tool [39].

The prepared structures were then subjected to an all-atom unrestrained molecular dynamics simulation in explicit solvent using GPU based PMEMD programme provided with Amber 12 [21,40]. Protein structures were parameterized and represented by ff03 variant of AMBER force field [41]. The tLeap module integrated with Amber 12 was used to add hydrogen atoms and counter ions for neutralization. The geometry and charges of the ligands were optimized with Gaussian 09 at HF/6-31G* level [42]. Finally

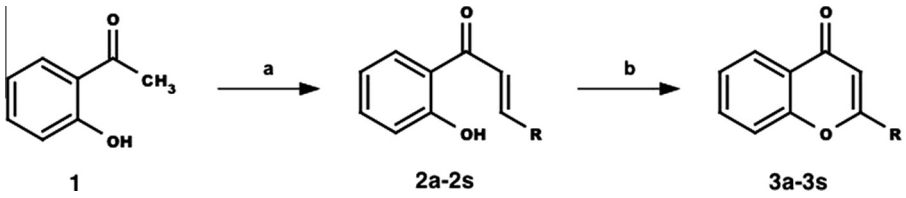

Scheme 1. Reagents and conditions: (a) R-CHO, aq. NaOH (60%), EtOH, 48 h, rt; (b) DMSO, I_2, reflux, 2 h.

ANTECHAMBER module was used to add partial atomic charges for the ligands using restrained electrostatic potential procedure (RESP) [43]. All systems were immersed in a orthorhombic box of TIP3P water molecules such that no atom of either protein or ligand was within 8 Å from any side of the box [44]. The partial mesh Ewald (PME) method was employed to calculate long range electrostatic potentials with a direct space and vdW cut-off of 12 Å [45]. All the systems were initially minimized for 1000 steps of steepest descent followed by 1000 steps of conjugate gradient with a restrained potential of 500 kcal/mol Å^2 applied to the solute. A further 100 steps unrestrained minimization of the all the systems were carried out for 1000 steps using conjugate gradient algorithm. Prior to minimization, a canonical ensemble MD simulation were carried out for 50 ps, with gradual heating from 0 K to 300 K with a harmonic restrained of 5 kcal/mol Å^2 and a Langevin thermostat with a random collision frequency of 1/ps. The prepared systems were subsequently equilibrated at 300 K using a NPT ensemble for 500 ps with no restrained imposed and the pressure was maintained at 1 bar. The SHAKE algorithm [46] was applied to constrain all bond lengths involving hydrogen at their equilibrium distance, a 2 fs time step and SPFP precision model [47] was used for all MD runs. Finally a 10 ns production MD run was performed for all the systems in a NPT ensemble [48] with a pressure of 1 bar and a coupling constant of 2 ps. Resultant coordinates were saved and analyzed in every 1 ps. Further analysis of trajectories (RMSD, potential energy) was performed using PTRAJ module implemented in Amber 12.

MM-GBSA based end-point energy calculation was performed to understand free energy differences between two different states [49–52]. Understanding of binding free energy profile provides an energetic insight into the process of binding. In this study the binding free energies of compound **3d** and **3j** bound with both MAO-isoforms were calculated using 1000 snapshots taken from 10 ns MD trajectory at 10 ps intervals. The binding free energy for analysis was carried out by the following set of equations:

$$\Delta G_{bind} = G_{complex} - (G_{receptor} + G_{ligand}) \quad (1)$$

$$\Delta G_{bind} = E_{gas} + G_{sol} - T\Delta S \quad (2)$$

$$E_{gas} = E_{int} + E_{vdw} + E_{ele} \quad (3)$$

$$G_{sol} = G_{GB} + G_{SA} \quad (4)$$

$$G_{SA} = \gamma SASA \quad (5)$$

where ΔG_{bind} is the total binding free energy, $G_{receptor}$ and G_{ligand} correspond to the energies of protein and ligand respectively. E_{gas} is the gas-phase energy; E_{int} is the internal energy; and E_{ele} and E_{vdW} are the Coulomb and Van der Waals energies, respectively. The solvation free energy, denoted by G_{sol}, can be decomposed into polar and nonpolar contribution states. The polar solvation contribution, G_{GB}, is determined by solving the GB equation, whereas, G_{SA}, the nonpolar solvation contribution is estimated from the solvent accessible surface area (SASA) determined using a water probe radius of 1.4 Å. T and S correspond to temperature and total solute entropy, respectively. Understanding of the binding free energy will help in understanding the selectivity of compound **3d** and **3j** towards MAO-A or MAO-B respectively.

3. Results and discussion

3.1. Chemistry

All the compounds were synthesized according to the reactions outlined in Scheme 1. Chalcones (**2a–2s**) were prepared through Claisen–Schmidt condensation of appropriate aromatic/heteroaromatic aldehydes with 2′-hydroxyacetophenone in 60% aqueous ethanolic sodium hydroxide solution. The final products (**3a–3s**) were obtained by refluxing chalcones (**2a–2s**) with iodine, dimethylsulfoxide (DMSO). Chalcones were identified by comparing their melting point with that of melting point reported in the literature and by IR spectra. IR peaks due to α,β-carbonyl group and phenolic hydroxyl group were displayed in the ranges 1610–1699 cm^{-1} and 3025–3396 cm^{-1}; respectively. Final compounds (**3a–3s**) were characterized by ^{1}H NMR, ^{13}C NMR and ESI-MS spectroscopy. Proton in 3rd position of chromenone appeared as a singlet between δ 6.6 and δ 7.10, methyl protons (**3k**) appeared as a singlet at δ 2.2, methoxy protons (**3g–3j**) appeared as singlet between δ 3.80–3.99 and hydroxyl proton (**3d–3f**) appeared as singlet between δ 8.15–12.5. ^{13}C NMR displayed carbonyl carbon (**3f**, **3q**) between δ 177–178. Mass spectra of compounds **3l-3s** displayed $(M+1)^+$ peak.

3.2. Biochemistry

All the compounds were screened for their hMAO inhibitory activity using recombinant hMAO-A and hMAO-B (Table 1). Sixteen compounds (**3a**, **3c**, **3e–3i**, **3j–3p**, **3r**, **3s**) were found to be selective towards hMAO-B, while one compound (**3d**) was selective towards hMAO-A and other two (**3b and 3q**) were non-selective. Amongst the hMAO-B inhibitors, the most potent compound was **3j** (K_i for hMAO-B is 0.16 ± 0.01 μM). Compound **3j** also appeared as the most selective MAO-B inhibitor in this series with SI_{MAO-B} of 30.0, which is comparable to that of Selegiline, the well-known selective MAO-B inhibitor (SI_{MAO-B} = 35.0). Compound **3d**, having 2-OH-C_6H_4 group at R position of the molecule, inhibited hMAO-A potently and selectively (K_i hMAO-A is 0.52 ± 0.03 μM; SI_{MAO-A} is 11.5). Fig. 1 displays the SI for MAO-A and MAO-B of the compounds **3a-3s**. All tested compounds inhibited the hMAO reversibly. Table 2 indicated the reversibility of hMAO-B inhibition with the compounds **3a–3s**. Compound **3d**, which inhibited hMAO-A reversibly is not included in the Table 2. The percentage inhibition (%) of hMAO-A of compound **3d** (200 nM) was calculated as 89.05 ± 5.68 and 8.44 ± 0.61 before and after washing, respectively whereas the percentage inhibition of hMAO-A inhibition (%) of moclobemide (200 nM) was calculated as 86.95 ± 4.77 and 9.02 ± 0.55 before and after washing, respectively.

A brief discussion of SAR with respect to MAO-B inhibition has been presented below. Amongst the fifteen selective MAO-B inhibitors, compounds having deactivating functional groups at *para* position of the phenyl ring (**3c**, **3l**, **3m**, **3n**) were found to be

Table 1
Human MAO inhibitory activity of compounds **(3a–3s)**.

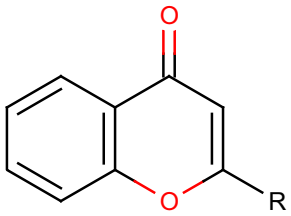

Compound	R-	Experimental		Exp MAO-B SI[a]	Exp MAO-A SI[a]	Inhibition type	Reversibility	MAO-Selectivity
		K_i value MAO-A (μM)[b]	K_i value MAO-B (μM)[b]					
3a	C_6H_5	2.50 ± 0.12	1.06 ± 0.09	2.4	0.4	Competitive	Reversible	MAO-B selective
3b	2-Cl-C_6H_4	1.90 ± 0.15	1.20 ± 0.10	1.6	0.6	Competitive	Reversible	Non-selective
3c	4-Cl-C_6H_4	3.90 ± 0.20	0.60 ± 0.04	6.5	0.2	Competitive	Reversible	MAO-B selective
3d	2-OH-C_6H_4	0.52 ± 0.03	5.98 ± 0.26	0.1	11.5	Competitive	Reversible	MAO-A selective
3e	3-OH-C_6H_4	3.02 ± 0.21	0.80 ± 0.04	3.8	0.3	Competitive	Reversible	MAO-B selective
3f	4-OH-C_6H_4	5.06 ± 0.21	1.05 ± 0.09	4.8	0.2	Competitive	Reversible	MAO-B selective
3g	2-OMe-C_6H_4	3.22 ± 0.25	1.65 ± 0.11	2.0	0.5	Competitive	Reversible	MAO-B selective
3h	3-OMe-C_6H_4	1.99 ± 0.13	0.86 ± 0.07	2.3	0.4	Competitive	Reversible	MAO-B selective
3i	4-OMe-C_6H_4	2.64 ± 0.18	1.80 ± 0.15	1.5	0.7	Competitive	Reversible	MAO-B selective
3j	3,4-OMe-C_6H_3	4.80 ± 0.10	0.16 ± 0.01	30.0	0.0	Competitive	Reversible	MAO-B selective
3k	4- Me-C_6H_4	3.32 ± 0.20	0.99 ± 0.05	3.4	0.3	Competitive	Reversible	MAO-B selective
3l	4-NO_2-C_6H_4	0.84 ± 0.05	0.20 ± 0.01	4.2	0.2	Competitive	Reversible	MAO-B selective
3m	4-CN-C_6H_4	8.21 ± 0.55	0.90 ± 0.05	9.1	0.1	Competitive	Reversible	MAO-B selective
3n	4-Br-C_6H_4	2.00 ± 0.16	0.52 ± 0.04	3.8	0.3	Competitive	Reversible	MAO-B selective
3o	Naphth-1-yl	0.80 ± 0.05	0.39 ± 0.02	2.1	0.5	Competitive	Reversible	MAO-B selective
3p	Naphth-2-yl	2.55 ± 0.20	1.30 ± 0.11	2.0	0.5	Competitive	Reversible	MAO-B selective
3q	Anthracen-9-yl	1.88 ± 0.09	1.15 ± 0.12	1.6	0.6	Competitive	Reversible	Non-selective
3r	Thiophen-2-yl	6.44 ± 0.51	2.91 ± 0.20	2.2	0.5	Competitive	Reversible	MAO-B selective
3s	Pyridin-3-yl	5.93 ± 0.37	1.90 ± 0.16	3.1	0.3	Competitive	Reversible	MAO-B selective
Selegiline	–	5.70 ± 0.05	0.16 ± 0.01	35.63	0.03	Competitive	Irreversible	MAO-B selective
Moclobemide	–	0.03 ± 0.01	1.40 ± 0.11	0.02	46.66	Competitive	Reversible	MAO-A selective

[a] Selectivity index calculated with Experimental K_i values: It was calculated as K_i (MAO-A)/K_i (MAO-B) for MAO-B and K_i (MAO-B)/K_i (MAO-A) for MAO-A. Selectivity towards MAO isoforms increases as the corresponding SI decreases.
[b] Each value represents the mean ± SEM of three independent experiments.

Table 2
Reversibility of hMAO-B inhibition with the compounds **3a–3s**.

Compounds (200 nM)	hMAO-B inhibition[a] (%)		
	Before washing	After washing	Reversibility
3a	84.50 ± 4.91	9.68 ± 0.65	Reversible
3b	80.06 ± 4.28	8.68 ± 0.55	Reversible
3c	90.76 ± 5.88	7.89 ± 0.41	Reversible
3e	87.00 ± 5.22	8.18 ± 0.47	Reversible
3f	87.65 ± 4.30	8.00 ± 0.69	Reversible
3g	80.02 ± 4.39	8.05 ± 0.70	Reversible
3h	85.81 ± 5.06	9.89 ± 0.80	Reversible
3i	80.12 ± 5.33	8.56 ± 0.58	Reversible
3j	92.19 ± 5.06	6.94 ± 0.42	Reversible
3k	86.90 ± 5.54	8.88 ± 0.55	Reversible
3l	88.22 ± 5.13	7.95 ± 0.48	Reversible
3m	89.00 ± 4.12	6.99 ± 0.39	Reversible
3n	87.35 ± 5.28	7.75 ± 0.55	Reversible
3o	85.90 ± 5.16	8.96 ± 0.80	Reversible
3p	84.13 ± 5.22	8.90 ± 0.71	Reversible
3q	78.90 ± 4.10	8.10 ± 0.60	Reversible
3r	82.44 ± 5.02	9.00 ± 0.54	Reversible
3s	85.66 ± 4.90	8.95 ± 0.57	Reversible
Selegiline	50.05 ± 3.11	48.97 ± 2.86	Irreversible

[a] Each value represents the mean ± S.E.M of three experiments.

selective and potent inhibitors of hMAO-B compared with compound having unsubstituted phenyl ring (**3a**). Strength of deactivating group was designated as (NO_2 > Br > Cl > CN) and well correlates with potency. Cyano group, being stronger than halogens, exhibited lesser potency due to difference in interaction with the protein, MAO-B (see Section 3.3). But the selectivity towards MAO-B ($SI_{MAO-B} = Ki_{MAO-A}/Ki_{MAO-B}$) was found to be in reverse order. Similarly compounds with activating functional group at *meta* position of the phenyl ring (**3e**, **3h**) were also found to be better than **3a** but definitely not better than compounds with deactivating functional groups at *para* position (**3c**, **3l**, **3m**, **3n**). These two compounds (**3e**, **3h**) did not displayed significant effect on

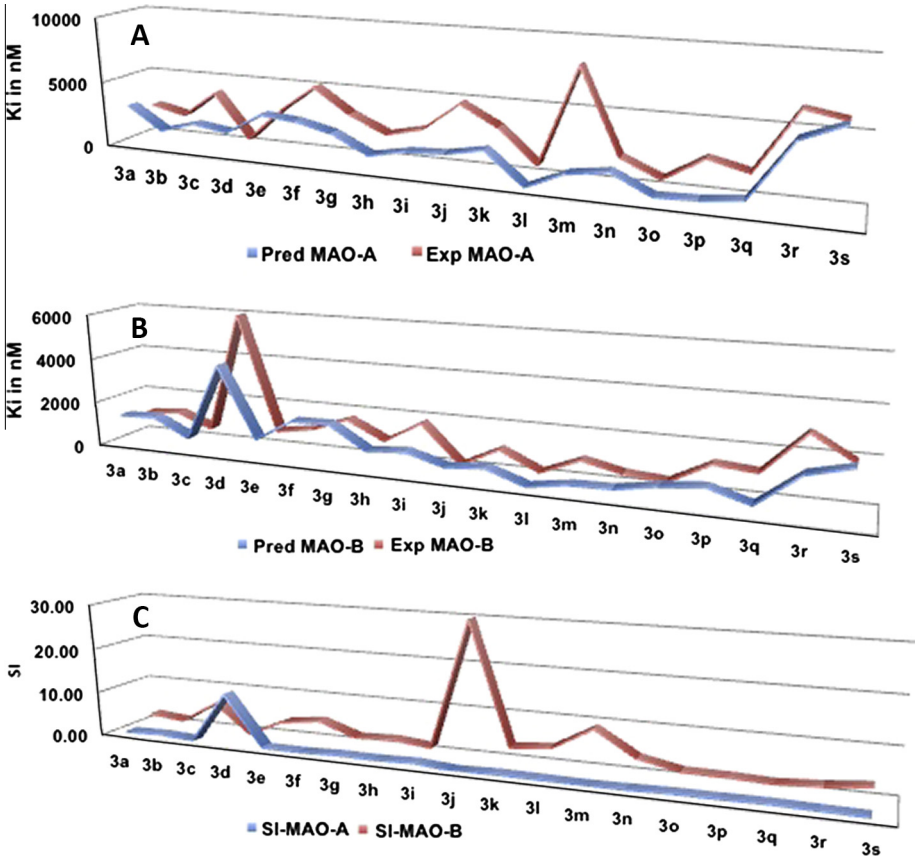

Fig. 1. Predicted K_i vs Experimental K_i (A and B) and SI (C) Plot against MAO-isoforms.

Table 3
Total binding free energy profile of compound **3d** and **3k** with MAO-isoforms.

Complex	E_{elec}	E_{vdW}	ΔG_{gas}	ΔG_{solv}	ΔG_{bind}
3d-MAO-A	−12.3188 ± 0.1017	−67.8562 ± 0.1285	−80.3953 ± 0.2019	20.6595 ± 0.1063	−59.5155 ± 0.2069
3d-MAO-B	−9.3756 ± 0.1097	−56.6836 ± 0.2185	−65.8738 ± 0.1996	16.6729 ± 0.09689	−49.3863 ± 0.2095
3j-MAO-A	−10.1897 ± 0.1586	−70.9590 ± 0.2246	−80.1658 ± 0.2002	20.2647 ± 0.1048	−60.9011 ± 0.2695
3j-MAO-B	−15.4189 ± 0.1009	−79.53674 ± 0.1586	−95.3066 ± 0.2864	24.1065 ± 0.1151	−70.1468 ± 0.2182

selectivity towards MAO-B. Compound **3j** (R = 3,4-di-OCH_3) was found to be most potent MAO-B inhibitor with best selectivity index of all the twenty compounds studied. These differences may be due to difference in binding mode rather than simply the strength of activating functional groups and additive effects due to their combination. Replacing phenyl ring with naphth-2-yl (**3p**), anthracen-9-yl (**3q**), thiophen-2-yl (**3r**) and pyridin-3-yl (**3s**) did not improved potency as well as selectivity towards MAO-B. Compound **3p** with naphth-1-yl replacing phenyl (**3a**) was found to be 2.7-fold better than **3a**, but displayed no great difference in Selectivity towards MAO-B. While Compound **3r** with antracen-9-yl replacing phenyl (**3a**) was found to be non-selective towards MAO-isoforms. Increasing bulkiness with addition of more rings gradually shifts MAO-B selective → Non-selective and may further be towards MAO-A. Further Molecular docking analysis was carried out to understand the interactions at molecular level that are responsible for potency and selectivity.

3.3. Molecular docking study

Molecular docking study was performed with the above-mentioned protocol (see Section 2.4) to understand the molecular level understanding of compound **3d** with MAO-A and compound **3j** with MAO-B. Binding mode analysis of compound **3d** with MAO-A (Fig. 2A) has revealed three H-bonding interaction viz., (i) hydroxyl hydrogen of **3d** with side-chain hydroxyl oxygen of SER209, (ii) hydroxyl oxygen of **3d** with backbone amino hydrogen of SER209 and (iii) chromenone ring oxygen with hydroxyl hydrogen of TYR444. The o-hydroxy phenyl group at 2nd position of chromenone also establishes pi-pi interaction with TRP441. These interactions kept pocket1 (Aromatic cage: FAD, TYR407, TYR444) unoccupied, pocket 3 (ILE180, ILE335, LEU337, MET350, PHE352) partially occupied by chromenone benzene ring and pocket 2 (GLY71, GLN74, ARG206, ILE207, PHE208, GLU216, TRP441) partially occupied by o-hydroxy phenyl ring at 2nd position of chromenone. All the other compounds with activating functional group **3e**-**3k** that are showing selectivity towards MAO-B binds differently with MAO-A. The chromenone benzene ring was accommodated in pocket 2 while phenyl ring at the 2nd position of chromenone ring in pocket 3. This is mainly due to the position and bulkiness of the substitution in the phenyl ring at the 2nd position of chromenone and relatively polar nature of the pocket 2 (compared with pocket 1 and 3). Polar character of pocket 2 is due to the amino acids: GLN74, ARG206, GLU216 and TRP441

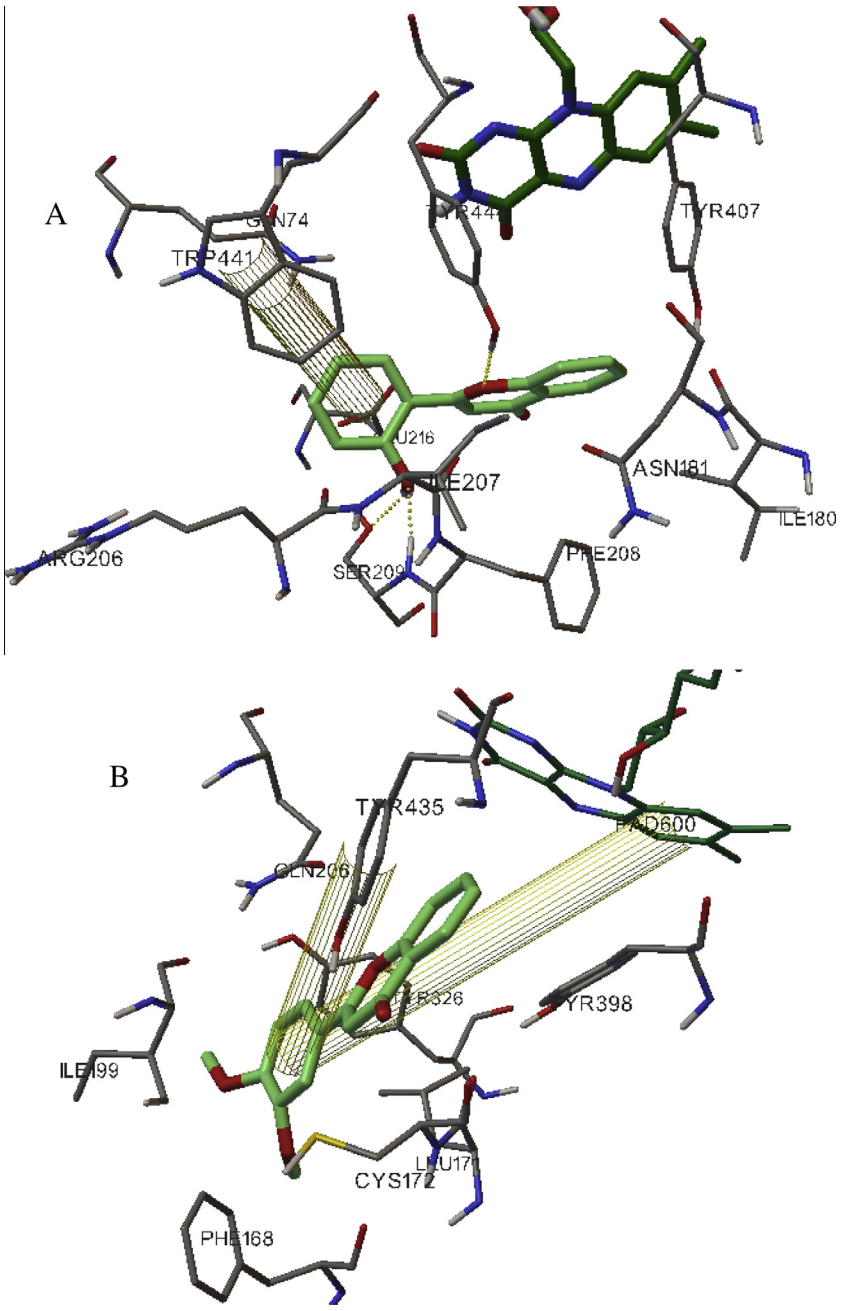

Fig. 2. (A) Interaction of compound **3d** with human MAO-A (PDB Code: 2BXR); (B) Interaction of compound **3j** with human MAO-B (PDB Code: 2BYB).

and is slightly electropositive due to GLN74, ARG206 and TRP441. This makes this pocket suitable for fragments with polar and electronegative in nature. These factors favored the establishment of (i) H-bonding interaction between chromenone carbonyl oxygen and backbone amino hydrogen of SER209 and (ii) pi–pi interaction between chromenone benzene ring with PHE352. The VdW interaction of **3d** is thus less than compounds **3e**–**3k**, but the difference in binding mode with favourable H-bonding and Electrostatic interaction makes the molecule potent than their counterparts (Table 2).

Binding mode analysis of compound **3j** with MAO-B (Fig. 2B) has revealed pi-pi interaction between phenyl ring at 2nd position of chromenone and TYR435 and FAD. The benzene ring of chromenone is comfortably accommodated in aromatic cage (FAD, TYR398, TYR435), while phenyl ring at 2nd position of the chromenone having two-methoxy substitution is placed in the narrow hydrophobic tunnel leading to solvent exposed entrance. Whereas the analysis of compounds containing deactivating functional groups at *para* position of phenyl ring (**3c**, **3l**–**3n**) at 2nd position of chromenone revealed difference in binding mode. In all the cases the phenyl ring carrying deactivating functional group is conveniently accommodated in aromatic cage and orienting the benzene ring of chromenone towards hydrophobic tunnel. The potent one amongst the four, **3l**, shows pi-pi interaction between chromenone benzene ring and TYR435. Compounds **3c** and **3m** displayed two pi-pi interaction, one between benzene ring of chromenone and TRY435 and the other between phenyl ring at 2nd position of chromenone and TYR435. While, the least potent one

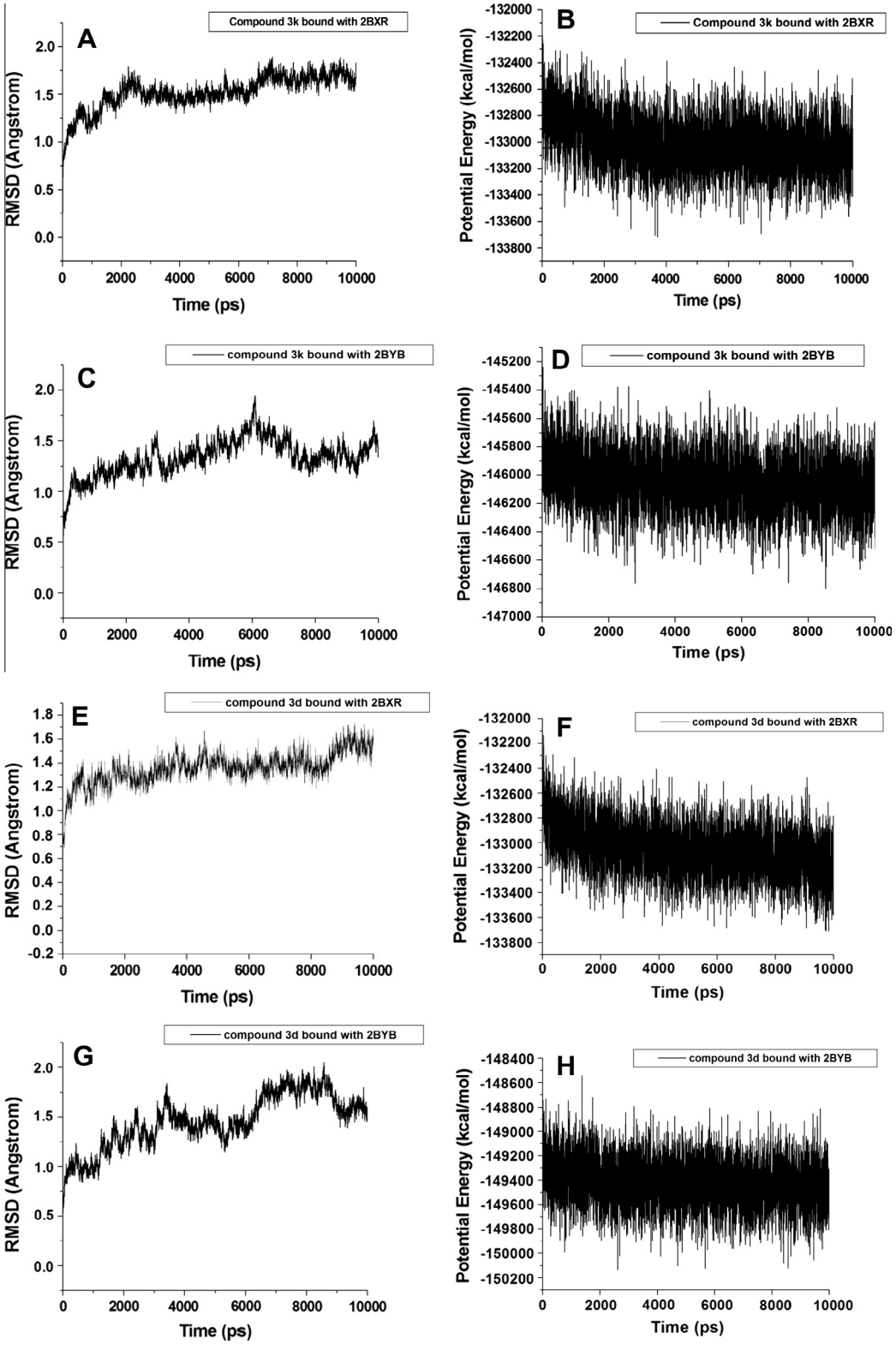

Fig. 3. Potential energy and RMSD vs Time curves for compounds **3d** and **3j** with both isoforms of MAO.

shows pi-pi interaction between phenyl rings at 2nd position of chromenone and TYR435.

The observations clearly indicated that the nature and position of the substituents determines the orientation of the molecule inside the active site of MAO-isoforms and in turn determines the potency and selectivity.

3.4. Molecular dynamics simulation

Molecular docking sometimes leads to artifacts [53]. Molecular dynamics (MD) simulation proven as a useful tool to understand the stability of the docked complexes as well as the free energy profile of ligand–protein complexes. It was observed from the

potential energy and RMSD plots that all the systems were well stabilized after a 10 ns MD simulation (Fig. 3). Also the RMSD and potential energy parameters were well converged over the time which made all systems ideal for a MM-GBSA based binding free energy analysis. MD based binding free energy analysis proven as a useful tool to understand ligand affinity towards receptor, which often co-relates highly with the experimental activity profile. Table 3 presents binding free energy profile of compound **3j** which clearly suggests the selectivity of compound **3j** towards MAO-B. The total binding free energy, ΔG_{bind} of compound **3j** found to be −70.1468 kcal/mol and −60.9011 kcal/mol with MAO-B and MAO-A respectively. Also other components of the free energy profile such as van der Waals, electrostatics, solvation and ΔG_{gas} were significantly higher in case compound **3j**- MAO-B complex. These large differences in binding free energy profile (~10 kcal/mol) further justify the selectivity of compound **3j** towards MAO-B, which was in accordance with the experimental data, which showed the MAO-B selectivity of compound **3j** (MAO-B = K_i (μm) value 0.16 ± 0.01, MAO-A = K_i (μm) value 4.80 ± 0.10). Whereas, binding free energy profile of compound **3d** (Table 3) suggests its selectivity towards MAO-A, which is in great accordance with the experimental data. The total binding free energy (ΔG_{bind}) of compound **3d** found to be −59.5155 kcal/mol and −49.3863 kcal/mol in complexes with MAO-A and MAO-B respectively. Similar trend in difference in all other free energy components were observed which contributed to the total binding energy (Table 3). The results indicated in the binding free energy profile highly correspond to the experimental selectivity of compound **3d** and compound **3j** towards MAO-A and MAO-B respectively.

Acknowledgments

Author was thankful to Birla Institute of Technology for providing financial support as an Institute Fellow. Also acknowledgement to Dr. Reddys Institute of Life Science, Hyderabad for spectral characterization.

Authors acknowledge Ross Walker of San Diego Supercomputer Center & Department of Chemistry and Biochemistry, University of California for providing GPU based super fast computational resources and School of Health Sciences, University of KwaZulu-Natal, Westville for technical and financial support.

Appendix A. Supplementary material

Supplementary data associated with this article can be found, in the online version, at http://dx.doi.org/10.1016/j.bioorg.2014.11.008.

References

[1] G. Collins, M. Sandler, E. Williams, M. Youdim, Nature 225 (1970) 817–820.
[2] M. Youdim, G. Collins, M. Sandler, A.B. Jones, C. Pare, W. Nicholson, Nature 236 (1972) 225–228.
[3] D. Horwitz, W. Lovenberg, K. Engelman, A. Sjoerdsma, JAMA, J. Am. Med. Assoc. 188 (13) (1964) 1108–1110.
[4] M. Yamada, H. Yasuhara, Neurotoxicology 25 (1) (2004) 215–221.
[5] F. Chimenti, R. Fioravanti, A. Bolasco, P. Chimenti, D. Secci, F. Rossi, M. Yanez, F. Orallo, F. Ortuso, S. Alcaro, J. Med. Chem. 52 (9) (2009) 2818–2824.
[6] S.J. Robinson, J.P. Petzer, A. Petzer, J.J. Bergh, A.C.U. Lourens, Bioorg. Med. Chem. Lett. 23 (17) (2013) 4985–4989.
[7] D. Secci, A. Bolasco, P. Chimenti, S. Carradori, Curr. Med. Chem. 18 (33) (2011) 5114–5144.
[8] L.-P. Guan, L.-M. Tang, C.-Y. Pan, S.-L. Zhao, S.-H. Wang, Neurochem. Res. 39 (2) (2014) 313–320.
[9] X. Sui, Y.-C. Quan, Y. Chang, R.-P. Zhang, Y.-F. Xu, L.-P. Guan, Med. Chem. Res. 21 (7) (2012) 1290–1296.
[10] D. Zhao, Y. Zhang, Z. Zheng, Shizhen Guoyi Guoyao 21 (5) (2010) 1115–1116.
[11] X. Liu, C.-B. Chan, S.-W. Jang, S. Pradoldej, J. Huang, K. He, L.H. Phun, S. France, G. Xiao, Y. Jia, H.R. Luo, K. Ye, J. Med. Chem. 53 (23) (2010) 8274–8286.
[12] X. Liu, C.-B. Chan, Q. Qi, G. Xiao, H.R. Luo, X. He, K. Ye, J. Med. Chem. 55 (19) (2012) 8524–8537.
[13] Y. Zhang, K. Wang, Z. Zhan, Y. Yang, Y. Zhao, Tetrahedron Lett. 52 (24) (2011) 3154–3157.
[14] F. Chimenti, F. Cottiglia, L. Bonsignore, L. Casu, M. Casu, C. Floris, D. Secci, A. Bolasco, P. Chimenti, A. Granese, J. Nat. Prod. 69 (6) (2006) 945–949.
[15] F. Chimenti, R. Fioravanti, A. Bolasco, P. Chimenti, D. Secci, F. Rossi, M. Yáñez, F. Orallo, F. Ortuso, S. Alcaro, Bioorg. Med. Chem. 18 (3) (2010) 1273–1279.
[16] S.-J. Lee, H.-Y. Chung, I.-K. Lee, S.-U. Oh, I.-D. Yoo, Food Sci. Biotechnol. 9 (3) (2000) 179–182.
[17] X.H. Han, S.S. Hong, J.S. Hwang, M.K. Lee, B.Y. Hwang, J.S. Ro, Arch. Pharmacal Res. 30 (1) (2007) 13–17.
[18] Maestro-8.5 User Manual, Schrodinger LLC, 2008, https://www.schrodinger.com//AcrobatFile.php?type=supportdocs&type2=&ident=236.
[19] G.M. Morris, R. Huey, W. Lindstrom, M.F. Sanner, R.K. Belew, D.S. Goodsell, A.J. Olson, J. Comput. Chem. 30 (16) (2009) 2785–2791.
[20] E.F. Pettersen, T.D. Goddard, C.C. Huang, G.S. Couch, D.M. Greenblatt, E.C. Meng, T.E. Ferrin, J. Comput. Chem. 25 (13) (2004) 1605–1612.
[21] D. Case, T. Darden, T. Cheatham III, C. Simmerling, J. Wang, R. Duke, R. Luo, R. Walker, W. Zhang, K. Merz, Amber 12, User Manual, University of California, San Francisco 1(2) (2012) 3.
[22] A.W. Schuttelkopf, D.M. van Aalten, Acta Crystallogr. D Biol. Crystallogr. 60 (Pt 8) (2004) 1355–1363.
[23] J.M. Word, S.C. Lovell, J.S. Richardson, D.C. Richardson, J. Mol. Biol. 285 (4) (1999) 1735–1747.
[24] B. VishnuNayak, S. Ciftci-Yabanoglu, S.S. Jadav, M. Jagrat, B.N. Sinha, G. Ucar, V. Jayaprakash, Eur. J. Med. Chem. 69 (2013) 762–767.
[25] P. Kumar, M.S. Bodas, Org. Lett. 2 (24) (2000) 3821–3823.
[26] A.S. Zambare, J.N. Sangshetti, N.D. Kokare, D.B. Shinde, Chin. Chem. Lett. 20 (2) (2009) 171–174.
[27] J. Looker, W.W. Hanneman, J. Org. Chem. 27 (2) (1962) 381–389.
[28] F. Chimenti, E. Maccioni, D. Secci, A. Bolasco, P. Chimenti, A. Granese, S. Carradori, S. Alcaro, F. Ortuso, M. Yáñez, J. Med. Chem. 51 (16) (2008) 4874–4880.
[29] B.L. Shaw, T.H. Simpson, J. Chem. Soc. (1952) 5027–5032.
[30] M. Khoobi, M. Alipour, S. Zarei, F. Jafarpour, A. Shafiee, Chem. Commun. 48 (24) (2012) 2985–2987.
[31] D. Kim, K. Ham, S. Hong, Org. Biomol. Chem. 10 (36) (2012) 7305–7312.
[32] M.C. Anderson, F. Hasan, J.M. McCrodden, K.F. Tipton, Neurochem. Res. 18 (11) (1993) 1145–1149.
[33] M. Yáñez, N. Fraiz, E. Cano, F. Orallo, Biochem. Biophys. Res. Commun. 344 (2) (2006) 688–695.
[34] M.M. Bradford, Anal. Biochem. 72 (1) (1976) 248–254.
[35] F. Chimenti, S. Carradori, D. Secci, A. Bolasco, B. Bizzarri, P. Chimenti, A. Granese, M. Yáñez, F. Orallo, Eur. J. Med. Chem. 45 (2) (2010) 800–804.
[36] L. De Colibus, M. Li, C. Binda, A. Lustig, D.E. Edmondson, A. Mattevi, Proc. Natl. Acad. Sci. USA 102 (36) (2005) 12684–12689.
[37] J.L. Banks, H.S. Beard, Y. Cao, A.E. Cho, W. Damm, R. Farid, A.K. Felts, T.A. Halgren, D.T. Mainz, J.R. Maple, J. Comput. Chem. 26 (16) (2005) 1752–1780.
[38] G.M. Sastry, M. Adzhigirey, T. Day, R. Annabhimoju, W. Sherman, J. Comput. Aided Mol. Des. 27 (3) (2013) 221–234.
[39] M. Origin Inc., Northampton, Wellesley Hills, 1999.
[40] A.W. Götz, M.J. Williamson, D. Xu, D. Poole, S. Le Grand, R.C. Walker, J. Chem. Theory Comput. 8 (5) (2012) 1542–1555.
[41] K. Lindorff-Larsen, S. Piana, K. Palmo, P. Maragakis, J.L. Klepeis, R.O. Dror, D.E. Shaw, Proteins: Struct., Funct., Bioinf. 78 (8) (2010) 1950–1958.
[42] M. Frisch, G. Trucks, H. Schlegel, G. Scuseria, M. Robb, J. Cheeseman, J. Montgomery Jr., T. Vreven, K. Kudin, J. Burant, Gaussian Inc., Wallingford, CT, 2004.
[43] P. Cieplak, W.D. Cornell, C. Bayly, P.A. Kollman, J. Comput. Chem. 16 (11) (1995) 1357–1377.
[44] W.L. Jorgensen, J. Chandrasekhar, J.D. Madura, R.W. Impey, M.L. Klein, J. Chem. Phys. 79 (2) (1983) 926–935.
[45] U. Essmann, L. Perera, M.L. Berkowitz, T. Darden, H. Lee, L.G. Pedersen, J. Chem. Phys. 103 (19) (1995) 8577–8593.
[46] J.-P. Ryckaert, G. Ciccotti, H.J. Berendsen, J. Comput. Phys. 23 (3) (1977) 327–341.
[47] S. Le Grand, A.W. Götz, R.C. Walker, Comput. Phys. Commun. 184 (2) (2013) 374–380.
[48] H.J. Berendsen, J.P.M. Postma, W.F. van Gunsteren, A. DiNola, J. Haak, J. Chem. Phys. 81 (8) (1984) 3684–3690.
[49] P.A. Kollman, I. Massova, C. Reyes, B. Kuhn, S. Huo, L. Chong, M. Lee, T. Lee, Y. Duan, W. Wang, Acc. Chem. Res. 33 (12) (2000) 889–897.
[50] I. Massova, P.A. Kollman, Perspect. Drug Discovery Des. 18 (1) (2000) 113–135.
[51] V. Tsui, D.A. Case, Biopolymers 56 (4) (2000) 275–291.
[52] A. Onufriev, D. Bashford, D.A. Case, J. Phys. Chem. B 104 (15) (2000) 3712–3720.
[53] B.K. Shoichet, S.L. McGovern, B. Wei, J.J. Irwin, Hits, leads and artefacts from virtual and high throughput screening, Molecular Informatics: Confronting Complexity, May 13th–16th, 2002, Brozen, Italy.